https://doi.org/10.5194/egusphere-2025-2042
Preprint. Discussion started: 11 August 2025

Measurement report：Molecular characterization of organic aerosol in coastal environments using offline FIGAERO-I-CIMS

Yuping Chen[1,2,3], Lingling Xu[1,2*], Xiaolong Fan[1,2], Ziyi Lin[1,2,3], Chen Yang[1,2,3], Gaojie Chen[1,2,3], Ronghua Zheng[1,2], Youwei Hong[1,2], Mengren Li[1,2], Yanru Zhang[4], Jinsheng Chen[1,2*]

[1]State Key Laboratory of Advanced Environmental Technology, Institute of Urban Environment, Chinese Academy of Sciences, Xiamen 361021, China.

[2]Fujian Key Laboratory of Atmospheric Ozone Pollution Prevention, Institute of Urban Environment, Chinese Academy of Sciences, Xiamen 361021, China.

[3]University of Chinese Academy of Sciences, Beijing 100049, China

[4]Xiamen Environmental Monitoring Station, Xiamen 361021, China

* Corresponding author.

E-mail address: Jinsheng Chen (jschen@iue.ac.cn) and Lingling Xu (linglingxu@iue.ac.cn).

https://doi.org/10.5194/egusphere-2025-2042
Preprint. Discussion started: 11 August 2025

Abstract. Organic aerosol (OA), as a key component of particulate matter, exerts significant impacts on public health and the environment. However, understanding of molecular characterization of OA under diverse environments remains limited. This study employed offline FIGAERO-I-CIMS (Filter Inlet for Gases and Aerosols coupled with iodide-adduct Chemical Ionization Mass Spectrometry) to analyze the molecular composition of OA in $PM_{2.5}$ samples collected from a coastal city (urban and seaside sites) in Southeast China during spring 2024. A total of 737 and 768 CHOX compounds were identified at the urban and seaside sites, respectively. CHO compounds dominated in signal intensity (>70%) at both sites, while CHON were more abundant at the urban site and S-containing compounds at the seaside site. The weighted effective oxygen numbers (urban 0.82, seaside 0.85) indicated higher oxidation levels in coastal compounds. Seaside CHOX exhibited lower unsaturation, reduced aromaticity, and higher oxidation states. Categorization showed that urban OA was more influenced by aromatic compounds, whereas seaside OA contained higher proportions of aged aliphatic compounds. Two distinct pollution episodes were selected to investigate CHOX evolution. Case 1 (local accumulation) showed enhanced CHON signals through NO_3·-initiated nighttime oxidation that promoted Aliphatic Nitrates formation, whereas Case 2 (marine air masses) showed increased proportions of Aliphatic-like O-rich CHOX compounds (28% to 39%) via aqueous-phase processing probably under high humidity. These findings advance our understanding of OA molecular characteristics and chemical evolution under different environmental conditions.

https://doi.org/10.5194/egusphere-2025-2042
Preprint. Discussion started: 11 August 2025

1 Introduction

The chemical compositions of organic aerosol (OA) are highly complex, exerting distinct impacts on human health and the environment. Parts of OA are emitted directly from natural and anthropogenic sources, known as primary organic aerosols (POA). Additionally, gaseous precursors such as SO_2, NOx, and volatile organic compounds (VOCs) could be absorbed into atmospheric aerosol and undergo a series of chemical reactions to form secondary organic aerosol (SOA) (Putman et al., 2012; Qi et al., 2017; Xu et al., 2020). Current research has focused more on the quantification and the characteristic of bulk OA (Chazeau et al., 2021; Huang et al., 2014; Sun et al., 2018; Zhou et al., 2020). At the molecular level, OA remains not well understood due to its complex composition, consisting of numerous individual compounds with diverse volatility, functionality, and solubility, and its ultralow atmospheric concentration, which introduces large uncertainties in detection and compound-specific identification (Stark et al., 2017; Xu et al., 2017a; Yu et al., 2016; Zheng et al., 2021). Both anthropogenic and natural sources of OA exacerbate the challenge of their identification and quantification in molecular composition (Daellenbach et al., 2024). Several studies have characterized OA in different environments and have found significant variations in OA molecular composition (Chen et al. 2020; Siegel et al. 2021; Zhang et al. 2024). For example, CHO and CHON compounds dominated urban OA, while S-containing compounds were more abundant in marine aerosols (Siegel et al. 2021; Xin et al. 2024). These studies illustrate that aerosol sources and atmospheric processes can significantly affect the molecular composition of OA. Therefore, accurate OA molecular composition and characterization analyses are essential for advancing the understanding of OA formation mechanisms and providing critical insights into aerosol control strategies (Redman et al., 2002; Wan et al., 2020).

Hard ionization techniques, such as Aerosol Mass Spectrometer (AMS) and Aerosol Chemical Speciation Monitor (ACSM), which are commonly used for online observation of aerosol organic components, cannot provide molecular information of

https://doi.org/10.5194/egusphere-2025-2042
Preprint. Discussion started: 11 August 2025

individual compounds. In contrast, soft ionization techniques overcome this limitation by enabling observation of OA molecular compounds. The traditional methods such as Electrospray Ionization-Fourier Transform Ion Cyclotron Resonance Mass Spectrometry (ESI-FT-ICR MS) and Extractive Electrospray Ionization Mass Spectrometry (EESI-MS) have been successfully used to characterize OA compositions due to their ultrahigh mass accuracy and resolution (An et al., 2019; Cui et al., 2024; Gallimore et al., 2017; Jiang et al., 2016; Ning et al., 2023). With the development of instruments, ultra-high resolution mass spectrometry has been increasingly adopted in the field observation of OA at the molecular level (Daellenbach et al., 2024; Xin et al., 2024; Ye et al., 2021; Zheng et al., 2021). Among these, Filter Inlet for Gases and Aerosols-Chemical Ionization Mass Spectrometry equipped with reagent ion iodide (FIGAERO-I-CIMS) has emerged as a promising technology to detect organic compounds with high acidity or polarity in OA in recent years (Lee et al. 2014; Lopez-Hilfiker et al. 2014; Bianchi et al. 2019; Du et al., 2022). FIGAERO-I-CIMS performs direct thermal desorption of filter samples, which reduces potential sample or compositional losses associated with conventional pretreatment procedures. Compared to ESI-FT-ICR MS, the OA compounds detected by FIGAERO-I-CIMS were more oxidized and saturated (Xin et al., 2024).

FIGAERO-I-CIMS can operate in both online and offline modes. At present, the longest known online operation was a seven-month observation conducted by Daellenbach et al. (2024) in Beijing. However, this prolonged operation faced some deficiencies, as the stability and airtightness of the instrument deteriorated over time. Compared to online mode, the offline mode of FIGAERO-I-CIMS lowers operating and maintenance costs and provides greater convenience for detecting samples from different environments within a short period of time. Recent studies have reported the employments of FIGAERO-I-CIMS in offline mode, e.g., at an urban background site during summer and winter in Stuttgart City, Germany (Huang et al. 2019), at an urban site in Beijing, China, under varying pollution levels (Cai et al. 2022), and on the route near the North Pole (Siegel et al. 2021). To date, research on the molecular

https://doi.org/10.5194/egusphere-2025-2042
Preprint. Discussion started: 11 August 2025

composition of OA under varying environmental conditions remains quite limited.

In this study, offline FIGAERO-I-CIMS was applied to characterize OA at the molecular level in $PM_{2.5}$ samples collected from two different sites (urban and seaside) in Xiamen, a coastal city in Southeast China, during spring 2024. Expanding on our earlier ACSM measurement, OA constituted 30-60% of fine aerosol in Xiamen, with SOA accounting for over 70% (Chen et al. 2022; Zhang et al. 2020). This work has three main objectives: (i) to characterize the molecular composition of OA and assess source impacts; (ii) to compare the physicochemical properties of CHOX compounds including saturation, oxidation state, and aromaticity, between urban and seaside environments; and (iii) to elucidate the chemical evolution processes of organic molecules through case studies. The findings will shed light on the influence of emission sources and atmospheric chemical processes on OA molecular composition in different environments.

2 Experimental Methods

2.1 $PM_{2.5}$ Sampling and Offline FIGAERO-I-CIMS Analysis

The study was conducted at two distinct sampling sites in Xiamen, a city situated along the southeast coast of China and characterized by a subtropical marine monsoon climate. The urban site was situated at the Institute of Urban Environment, Chinese Academy of Sciences (24°26'N, 118°03'E). This site lies in proximity to major roads (Jimei Avenue and Haixiang Avenue) approximately 100 m away, experiencing high traffic density. The seaside site was located at the Xiamen Atmospheric Observation Supersite (24°28'N, 118°10'E), approximately 2.5 km from the coastline and 18.5 km from the urban site. Potential influence from shipping activities due to the vicinity of Xiamen Port may affect the seaside site. $PM_{2.5}$ was sampled during the spring season from 20 March to 30 April, 2024, with a sampling time of 23 hours from 10:00 a.m. to 9:00 a.m. the following day for each sample. A total of 38 and 32 filter samples were obtained from the urban and seaside sites, respectively, with one procedure blank used to assess potential contamination during sampling and transportation.

The offline filter sampling steps are similar to previous studies (Hong et al., 2018;

https://doi.org/10.5194/egusphere-2025-2042
Preprint. Discussion started: 11 August 2025

Hong et al., 2022). Briefly, a high-volume aerosol sampler (TH-1000 series, Tianhong Corp., Wuhan, China) was operated at a flow rate of 1.05 m^3 min^{-1} and particulate matter with a diameter of less than 2.5 μm was collected on pre-baked quartz fiber filters (18 cm × 23 cm). Before sampling, the quartz filters were wrapped in aluminum foil and burned in a muffle furnace for 4 h (temperature: 450 ℃) to remove residual carbon components from the filters. The burned quartz filters were conditioned in a constant temperature (25 ℃) and humidity (60%) chamber for 24 h, and then weighed using a balance. After sampling, the filter samples were stored at -20 ℃ before further chemical analysis. The field blank sample was taken following the same procedure without drawing air through the sampler.

$PM_{2.5}$ filter samples were analyzed by the FIGAERO-CIMS in offline mode with negative iodide (I^-) ions as the reagent (Aerodyne Research Inc., USA and Tofwerk AG, Switzerland). Heated and dry ultra-high-purity (UHP) N_2 was passed through a permeation tube containing liquid methyl iodide (CH_3I; Alfa Aesar, 99%) to an X-ray source (Tofwerk AG, P-type), producing I^- to charge the thermally desorbed compounds. Different from the sandwich method used in other studies (Cai et al., 2022; Cai et al., 2023; Xin et al., 2024), an area (1.85 cm^2) of the sample filters was punched and placed manually in the dedicated filter holder of FIGAERO directly. This larger area of filter membrane was used to enhance mass spectrometry signals due to the relatively low particle concentration in this study. More information was described in Text S1. A uniform temperature ramping protocol was applied for all filters, following four steps: (1) stabilization at 25 °C for 1 min; (2) heating from 25 °C to 200 °C in 24 min; (3) soaking at 200 °C for 15 min; and (4) cooling to 25 °C within 15 min. Two heating cycles were analyzed for each filter sample to assess the instrument background (Fig. S1). Meanwhile, parallel experiments were conducted to examine the effects of sampling and operation, with linear regression slopes ranging from 0.84 to 1.13 and the correlation coefficients upwards to 0.997 (Fig. S2).

2.2 Coordinated Observations

Simultaneous observations of atmospheric species were also carried out at the

https://doi.org/10.5194/egusphere-2025-2042
Preprint. Discussion started: 11 August 2025

same stations during the sampling campaign. The method of N_2O_5 concentration detected by online I-CIMS was described by Chen et al. (2024). The concentrations of water-soluble ions, including Na^+, NH_4^+, K^+, Ca^{2+}, Mg^{2+}, F^-, Cl^-, NO_3^{2-} and SO_4^{2-}, were measured by Ion Chromatography (Metrohm 883). OC and EC concentrations were detected by a Model-4 semi-continuous OC/EC aerosol analyzer (Sunset Laboratory Inc., USA). Black carbon (BC) at a wavelength of 880 nm was determined with a model AE-31 Aethalometer (Magee Co., USA). Additional measurements were obtained from instruments deployed at the sampling sites and nearby national air quality monitoring stations, located approximately 1 km and 2 km from the IUE and XS, respectively. Trace gases, i.e., carbon oxide (CO), ozone (O_3), sulfur dioxide (SO_2), and nitrogen oxides (NOx), were simultaneously measured by gas analyzers (Thermo Fisher Scientific, Waltham, MA, USA). Meteorological parameters, including wind speed (WS), wind direction (WD), temperature (T), and relative humidity (RH), were recorded by automatic weather observation station. Ultraviolet radiation (UV) was determined by a UV radiometer (KIPP & ZONEN, SUV5 Smart UV Radiometer). Comprehensive data for all measured parameters at both sites are summarized in Table S1.

2.3 Data Process and Analysis

The TofTools package (Junninen et al., 2010; version 6.11) based on MATLAB (MathWorks Inc.) was used to analyze offline FIGAERO-I-CIMS data. The majority of detected compounds fell within the m/z range of 200-500. These ions formed I^- adducts, i.e., $[M]I^-$, where M represents the original molecular formula of the analytes. Besides, a small proportion of compounds existed in other forms, such as losing a hydrogen (H) atom and combining with NO_3^- or HNO_3I^-. Mass calibration was performed using five calibrants: NO_3^- (m/z 61.99), I^-(m/z 126.91), H_2OI^- (m/z 144.92), HNO_3I^- (m/z 189.90), and I_3^- (m/z 380.71).

High-resolution peak fitting was performed on 1-minute averaged data, the signal intensity of each compound was subsequently normalized to the signal of reagent I^- and H_2OI^-. Signals of the first 1-min of ramping and the last 1-min of

https://doi.org/10.5194/egusphere-2025-2042
Preprint. Discussion started: 11 August 2025

soaking periods were excluded in order to minimize potential interference from temperature transitions (Cai et al., 2023), the calculation formula of the normalized signal for each compound i was as follows:

$$Normalized\_Signal_i = \frac{\int_{t=2}^{t=39} signal_i}{\int_{t=2}^{t=39} signal_{I^-} + \int_{t=2}^{t=39} signal_{H_2OI^-}} - \frac{\int_{t=57}^{t=99} signal_i}{\int_{t=57}^{t=94} signal_{I^-} + \int_{t=57}^{t=94} signal_{H_2OI^-}} \quad (1)$$

The detected molecules were classified into four categories based on their elemental composition: CHO (containing only C, H, and O elements), CHON (containing 1–2 N atoms in addition to C, H, and O elements), CHOS (containing only C, H, O, and S elements), and CHONS compounds (containing C, H, O, N, and S elements). In this study, CHOS and CHONS were collectively categorized as S-containing compounds. The sum of the four compound classes was denoted as CHOX, where X represents the possible presence of N, S, or both.

To characterize the properties of the OA compounds, the double bond equivalent (DBE), oxidation state of carbon atoms (OS_C), modified aromaticity index (AI_{mod}), and the effective number of oxygen atoms (O_{eff}) were calculated for the obtained molecular formulas. The DBE, which quantifies the number of rings and double bonds in a molecule (Koch and Dittmar, 2006), was calculated using Equation (2):

$$DBE = \frac{2 \times c + 2 - h + n}{2} \quad (2)$$

The OS_C was estimated according to Equation (3) described by Kroll et al. (2011):

$$OSc \approx 2 \times o/c - h/c \quad (3)$$

The AI_{mod} was first proposed by Koch and Dittmar (2006, 2016) to evaluate the aromaticity of compounds identified through high-resolution mass spectrometry. The index is calculated based on two parameters. DBE_{AI} is the DBE of molecular core structure, and C_{AI} is the number of carbon atoms in the core structure. AI_{mod} is defined as the DBE_{AI} to C_{AI} ratio, with the $AI_{mod} = 0$ when either $DBE_{AI} \leq 0$ or $C_{AI} \leq 0$ (Brege et al., 2018):

https://doi.org/10.5194/egusphere-2025-2042
Preprint. Discussion started: 11 August 2025

$$AI_{mod} = \frac{DBE_{AI}}{C_{AI}} = \frac{1 + c - 0.5 \times o - s - 0.5 \times (h + n)}{c - 0.5 \times o - s - n} \quad (4)$$

The O_{eff} was evaluated following Equation (5):

$$O_{eff} = o - 2 \times n - 3 \times s \quad (5)$$

In the aforementioned formulas, c, h, o, n, and s represent the number of C, H, O, N, and S atoms, respectively, in the molecular formulas of the corresponding compounds. The ratios DBE/C and O_{eff}/C indicate the degree of aromaticity and oxidation of compounds, respectively.

An intensity-weighted parameter (P_w) for CHOX compounds was calculated using Equation (6):

$$P_W = \sum (P_i \times I_i) / \sum I_i \quad (6)$$

where P represents the following parameters: DBE, DBE/C, O_{eff}/C, OSc, or AI_{mod}. P_i corresponds to the specific parameter value for individual compound i and I_i denotes the signal intensity of compound i. The weighted parameters for both sampling sites are summarized in Table S2.

3 Results and Discussion

3.1 Overview of the sampling period

During the sampling period, distinct differences in conventional air pollutants were observed between the urban and seaside sites. As shown in Table S1, primary-emitted and traffic-related pollutants like CO and NO*x* exhibited significantly higher concentrations at the urban site compared to the seaside site, while an opposite trend was observed for SO_2 concentrations. Additionally, the seaside site displayed enhanced O_3 concentrations and UVB intensity, indicating more favorable conditions for photochemical reactions. The average OC/EC ratio in $PM_{2.5}$ was 6.7 ± 4.4 at the seaside site, significantly higher than the urban site value of 4.0 ± 0.8 (t-test, p<0.001). Both sites exceeded the SOA formation indicator value (OC/EC = 2) proposed by Chow et al. (1996), indicating strong SOA production in the study area, particularly at the seaside site. In this study, a total of 737 and 768 organic molecules (CHOX) were

https://doi.org/10.5194/egusphere-2025-2042
Preprint. Discussion started: 11 August 2025

identified by FIGAERO-I-CIMS for the urban site and the seaside site, respectively. Significant correlations were observed between CHOX signal intensities and OC concentrations at both sites (R = 0.70 and 0.80, Fig. S3), demonstrating the reliability of the OA molecule detection method in this study. The number of identified molecules is comparable to that at a rural site in Southeast US (769 organic molecules, Chen et al., 2020) but lower than those observed in highly industrialized urban areas such as Beijing (939 molecules, Cai et al., 2022) and Guangzhou (815 molecules, Ye et al., 2021). These spatial differences highlight the significant influence of environmental conditions on OA molecular composition.

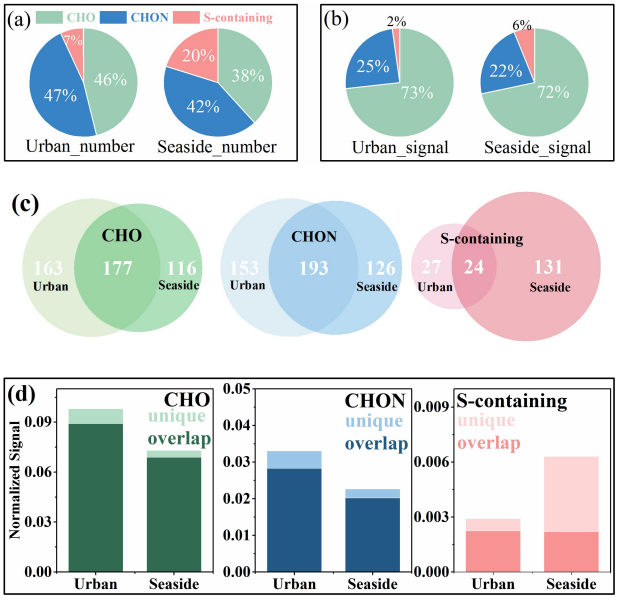

Fig. 1 Numbers (a) and signals intensity (b) proportion of CHO, CHON, and S-containing compounds in CHOX, Venn diagram of the number distribution of overlapping molecular formulas between sites (c), and average signals of overlapping and unique CHO, CHON, and S-containing compounds at both sites (d).

As described in the methodology section, the identified CHOX were classified into four groups. CHO and CHON compounds were predominant in quantity (Fig. 1a), accounting for 46% and 47% of the total CHOX at the urban site, and 38% and 42% at the seaside site, respectively. In terms of signal intensity, CHO and CHON

https://doi.org/10.5194/egusphere-2025-2042
Preprint. Discussion started: 11 August 2025

contributed over 70% and 20% to the total CHOX, respectively, at both sites (Fig. 1b). This observation is consistent with the well-documented predominance of CHO compounds across various environments, including urban areas (e.g., 65 ± 5% in Beijing) (Cai et al., 2022), rural areas (79.9 ± 5.2% on average in the Rhine river valley, Hyytiälä boreal forest, Finland, and Alabama, US; 87.7 ± 10.8% in Georgia, US) (Chen et al., 2020; Lopez-Hilfiker et al., 2016) and mountain sites (e.g., 66.2 ± 5.5% in Chacaltaya, Bolivia) (Bianchi et al., 2022). In addition, enhanced contributions of CHON compounds are consistently found at the urban sites, such as in Beijing (30 ± 5%) (Cai et al., 2022) and on average across Stuttgart and Karlsruhe, Germany and Delhi, India (27.1 ± 4.3%) (Haslett et al., 2023; Huang et al., 2019; Huang et al., 2024), strongly suggesting an association with urban NO*x* enrichment.

The molecular masses were identified within the range of m/z 200–500 (Fig. S4). The highest relative abundances, covering m/z 200–320, were found for CHO compounds, while CHON was mainly concentrated in the range of m/z 320–400. These characteristics are consistent with the results reported from Beijing, Wuhan, and Xi'an (Cai et al., 2022; Xin et al., 2024; Shang et al., 2024). As shown in Fig. 1d and S5, the signal intensities of CHO and CHON were steadily higher at the urban site, whereas the signals of S-containing compounds were more pronounced at the seaside site. These differences align with the elevated NO_2 at the urban location and the higher SO_2 measured at the seaside location during sampling (Table S1). Comparing CHOX chemical compounds at the two sites (Fig. 1c and S6), we found that over 50% of CHO and CHON molecules at both sites shared the same molecular formula, accounting for 86%–94% of total signals. Notably, the overlapping S-containing compounds constituted only a minor proportion of total S-containing species at the seaside site (35%). These results reveal distinct variations in OA composition between the urban and seaside sites, attributable to differences in anthropogenic emission influences. To further explore the discrepancies in CHOX compounds between the two sites, the characteristics and properties of CHOX were analyzed in detail.

3.2 Characteristics and Properties of CHOX Compounds

https://doi.org/10.5194/egusphere-2025-2042
Preprint. Discussion started: 11 August 2025

3.2.1 The Characteristics of CHOX Distribution

The bulk molecular formulas of CHOX compounds were determined as $C_{10.8}H_{13.7}N_{0.5}O_{5.4}S_{0.1}$ at the urban site and $C_{10.7}H_{14.4}N_{0.4}O_{5.4}S_{0.2}$ at the seaside site, with mean weighted effective oxygen numbers (O_{eff}/C) of 0.82 and 0.85, respectively, indicating the highly oxidized nature of these compounds in the coastal region. In comparison, the bulk CHOX composition at the seaside site exhibited a higher O/C ratio, fewer CHON compounds, and more S-containing compounds. The elevated CHON signal intensity at the urban site could be attributed to the high NO*x* concentrations from vehicle emissions, facilitating nitrogen-containing compound formation. In contrast, the enhanced S-containing compound signals at the seaside site likely resulted from marine-driven sources.

Figure 2 and S7 show the signal intensity and quantity distribution of CHO and CHON compounds as a function of carbon number. The distribution characteristics of CHO and CHON compounds were broadly consistent between the two sites. As shown in Fig. S7, the quantity of CHO compounds exhibited a normal distribution with carbon number, mainly concentrated in the ranges of 8–14 carbon and 4–6 oxygens, while the distribution of CHON compounds was relatively uniform, with a minor abundance peak at $C_{6–10}$ and $O_{5–6}$. In contrast to the quantity distribution, the signal intensity of CHO compounds decreased with increasing carbon number (Fig. 2a–b). Both sites exhibited significant signal contributions from O_4-CHO compounds, which likely correspond to dicarboxylic acid species. Oxalic acid (C_2) and succinic acid (C_4) were the most abundant species, followed by malonic acid (C_3). These low-molecular-weight dicarboxylic acids are typically associated with aqueous reactions (Lim et al., 2010). With increasing carbon number, the dominant oxygen content in CHO compounds shifted from O_4 to $O_{5–6}$. The signals of CHON compounds were predominantly concentrated in the $C_{3–10}$ range, with their oxygen content shifting from O_3 to $O_{5–7}$ as carbon number increased (Fig. 2c–d). Site-specific differences in compound distribution were observed. CHO and CHON compounds with high carbon content (>C_{10}) exhibited stronger signal intensities at the urban site

https://doi.org/10.5194/egusphere-2025-2042
Preprint. Discussion started: 11 August 2025

compared to the seaside site, with O_6-CHO and O_8-CHON species showing particular enhancement.

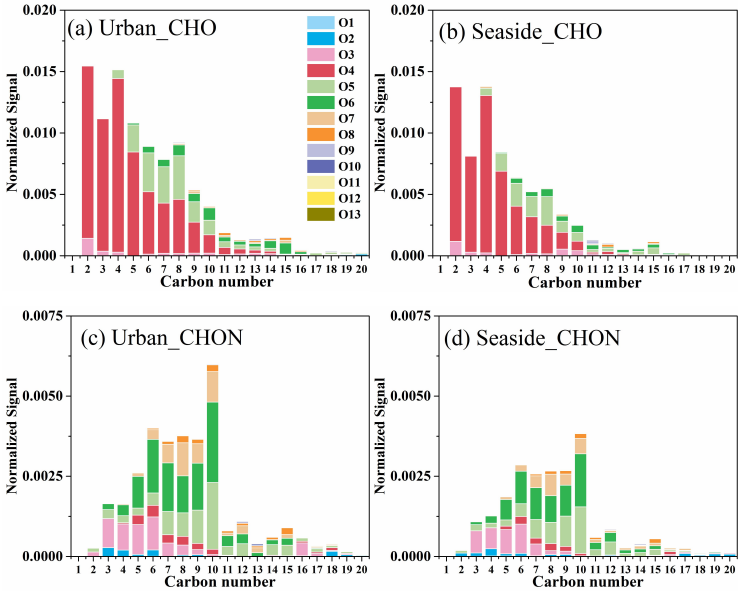

Fig. 2 Signal intensity of CHO and CHON categorized by the number of carbon atoms at the urban (a, c) and seaside (b, d) sites.

3.2.2 The Unsaturation, Oxidation State, and Aromaticity of CHOX Compounds

The double bond equivalent (DBE) characterizes the potential number of rings and double bonds in organic compound molecules. Quantitatively, CHOX compounds were predominantly distributed within the DBE range of 2–8 (Fig. S8). In terms of signal intensity (Fig. 3), CHO compounds exhibited significant contributions in the DBE = 2–4 range, while CHON compounds were concentrated in the DBE = 2–5 range. Compounds with DBE ≥ 6 showed higher signal contributions at the urban site (9%) than at the seaside site (7%). These highly unsaturated compounds may undergo oxidative transformation into higher molecular weight products, being particularly prone to photooxidation with oxidants like O_3-containing species to form of C=O bonds in carbonyls and carboxylic acids (Zhao et al., 2014). As shown in Table S2, the weighted-DBE values of CHOX compounds ranged from 2.32 to 3.68, which is close to the previously reported values (2.64–3.82) for urban and marine samples (Xin et al.,

https://doi.org/10.5194/egusphere-2025-2042
Preprint. Discussion started: 11 August 2025

2024). The urban site exhibited higher weighted-DBE values for CHOX compounds (3.25) compared to the seaside site (2.99) (Table S2), indicating distinct formation pathways. The highly unsaturated CHOX compounds likely derived from anthropogenic precursors such as aromatic VOCs and PAHs (Chen et al., 2014), whereas the more saturated components primarily originated from biogenic terpene compounds (Du et al., 2024; Chan et al., 2011; Nguyen et al., 2012; Noziere et al., 2010).

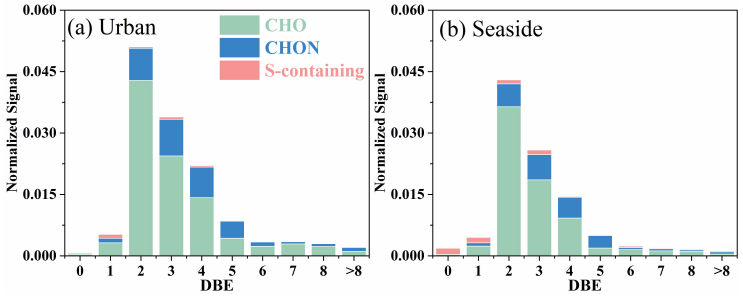

Fig. 3 Signal intensity of CHOX categorized by double bonds equivalent (DBE) at the urban site (a) and the seaside site (b).

DBE/C ratios greater than 0.7 generally indicate the presence of soot materials or oxidized polycyclic aromatic hydrocarbons (PAHs) (Cui et al., 2019). During the sampling period, while the signal proportions of compounds with DBE/C > 0.7 were comparable between the two sites (CHO: ~25%; CHON: ~16%), their number proportions were significantly higher at the urban site (CHO: 17%; CHON: 22%) than at the seaside site (CHO: 6%; CHON: 19%). Consistent with the above discussion, S-containing compounds with DBE/C > 0.7 exhibited higher proportions in both signal intensity and quantity at the urban site (24% and 26%, respectively) compared to the seaside site (14% and 10%, respectively). The systematically higher DBE/C ratios for OA compounds at the urban site suggest more contribution from soot materials and/or oxidized PAHs, which aligns with the observed EC concentrations (urban: 1.57 ± 0.80 μg m^{-3}; seaside: 0.91 ± 0.42 μg m^{-3}). The AI_{mod}, which reflects the minimum number of carbon-carbon double bonds and aromatic rings (Koch and Dittmar, 2006, 2016), was correspondingly higher at the urban site

https://doi.org/10.5194/egusphere-2025-2042
Preprint. Discussion started: 11 August 2025

(weighted-AI_{mod}=0.17) than at the seaside site (0.15), further supporting the greater contribution of aromatic species to urban OA.

The carbon oxidation state (OSc), a parameter introduced by Kroll et al. (2011), serves to quantify the oxidation degree of organic mixtures undergoing dynamic atmospheric processes. The weighted-OSc values of CHOX compounds were higher at the seaside site (0.55) than at the urban site (0.49) (Table S2), consistent with the aforementioned enhanced SOA formation at the seaside site. The van Krevelen (VK) diagrams (Fig. S9) revealed that homologue series such as $C_nH_{2n-x}O_4$ (where x=2,4,6) made significant contributions to CHOX compounds in this study. The elevated weighted-OSc values of seaside CHO compounds could be attributed to the strong signal intensities of low-carbon-number homologues, such as $C_nH_{2n-2}O_4$ and $C_nH_{2n-4}O_4$. In contrast to CHO compounds, both CHON and S-containing compounds exhibited higher weighted-OSc values at the urban site, indicating a more chemically aged state of N- and S-containing species. The increased weighted-OSc of urban CHON compounds mainly resulted from enhanced signals of highly oxidized species, such as $C_3H_5NO_6$ and $C_5H_7NO_6$. The relatively low weighted-OSc of seaside S-containing compounds was most likely associated with fresh sulfur emissions from local sources, including oceanic discharge and ship exhaust. This observation aligns with previous findings that S-containing compounds in primary organic sea spray aerosols are predominantly composed of fatty acids and other lipid molecules with lower oxidation degrees (Siegel et al., 2021). Additionally, the limited number of identified S-containing compounds may have artificially inflated the weighted-OSc values for urban S-containing compounds.

3.2.3 The Classification of CHOX Compounds

As shown in Fig. 4, CHOX compounds were categorized based on AI_{mod}, DBE, H/C, and O/C ratios. Low H/C ratios, combined with high DBE and AI_{mod} values indicate a high degree of unsaturation and the presence of aromatic structures. CHOX were classified into Aromatic-like and Aliphatic-like compounds based on AI_{mod} and H/C, following the methodology of Xin et al. (2024). Compounds with $AI_{mod} > 0.5$ or

https://doi.org/10.5194/egusphere-2025-2042
Preprint. Discussion started: 11 August 2025

$AI_{mod} \leq 0.5$ and H/C < 1.5 were defined as Aromatic-like compounds. Conversely, compounds with $AI_{mod} \leq 0.5$ and H/C ≥ 1.5 were defined as Aliphatic-like compounds (Coward et al., 2019). The categorical distribution of CHOX was generally consistent between the two sites, with Aromatic-like CHOX dominating over Aliphatic-like CHOX in signal intensity, indicating prevalent aromatic precursor contributions to OA formation across the study area.

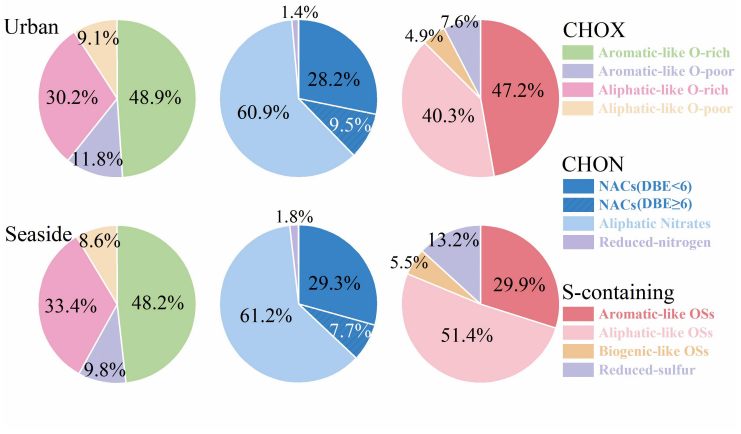

Fig. 4 Fraction of CHOX signal intensity categorized by different parameter.

Using an O/C threshold of 0.5, both Aromatic-like and Aliphatic-like CHOX were further subdivided into two subcategories, with O-rich (O/C > 0.5) compounds being more abundant than O-poor (O/C ≤ 0.5) compounds. The signal ratios of O-rich to O-poor compounds were higher at the seaside site for both categories. Specifically, the O-rich/O-poor ratio for Aromatic-like CHOX was 4.9 at the seaside site versus 4.1 at the urban site. Similarly, the ratio for Aliphatic-like CHOX was 3.9 at the seaside site compared to 3.3 at the urban site. These results are consistent with the findings of OC/EC ratios and OSc discussed earlier, suggesting that the seaside atmosphere is more conducive to the formation of highly oxidized organic compounds. Notably, the proportion of Aliphatic-like O-rich CHOX was significantly higher at the seaside site than at the urban site, aligning with a recent study that reported elevated levels of Aliphatic-like O-rich CHOX in marine-remote $PM_{2.5}$ (Xin et al., 2024). These findings demonstrate a consistent spatial pattern that urban OA is more influenced by

https://doi.org/10.5194/egusphere-2025-2042
Preprint. Discussion started: 11 August 2025

anthropogenic emissions, dominated by aromatic species, whereas marine-influenced OA exhibits higher proportions of aged, aliphatic compounds.

For CHON compounds, Aromatic-like compounds with O/N ≥ 2 and Aliphatic-like compounds with O/N ≥ 3 were categorized as Nitro-aromatic compounds (NACs) and Aliphatic Nitrates, respectively, while the remaining compounds were classified as Reduced-nitrogen compounds. The distribution patterns of CHON classifications were highly consistent between the two sites. Aliphatic-like CHON exhibited the highest signal proportion, followed by NACs, with Reduced-nitrogen compounds showing the lowest signal contribution. The most abundant compound in Aliphatic-like CHON was $C_{10}H_{15}NO_6$, accounting for 7.5% of total signals at both sites. Previous studies have demonstrated that $C_{10}H_{15}NO_6$ is produced through nitrate radical ($NO_3^{\cdot}$)-initiated oxidation of monoterpenes (e.g., limonene or β-pinene, $C_{10}H_{16}$) (Boyd et al., 2015; Faxon et al., 2018). Regarding NACs, $C_nH_{2n-7}O_xN$ homologues (e.g., $C_6H_5NO_3$, $C_8H_{11}NO_7$, and $C_7H_7NO_3$), likely originating from vehicle or combustion emissions, dominated the signal profiles at both sites. Notably, NACs with DBE ≥ 6 exhibited higher signal intensities at the urban site, primarily attributable to stronger influences from traffic- or combustion-related sources.

Following Lin et al. (2012) and Xie et al. (2020), S-containing compounds with O/S ≥ 4 were defined as organosulfates (OSs) and further divided into three subcategories: (1) Aromatic-like OSs ($AI_{mod} > 0.5$, or $AI_{mod} \leq 0.5$ with $H/C < 1.5$); (2) Aliphatic-like OSs ($AI_{mod} \leq 0.5$, $H/C \geq 1.5$, and $DBE \leq 2$); (3) Biogenic-like OSs ($AI_{mod} \leq 0.5$, $H/C \geq 1.5$, and $DBE > 2$). Compounds with $O/S < 4$ were classified as Reduced-sulfur compounds. Unlike CHO and CHON, the classification distribution of S-containing compounds showed marked differences between the two sites. At the urban site, Aromatic-like OSs dominated the signal profiles, followed by Aliphatic-like OSs. In contrast, the seaside site exhibited the highest signal proportion of Aliphatic-like OSs, primarily contributed by compounds such as $C_3H_6O_5S$, $C_3H_8O_5S$, and $C_4H_{10}O_5S$. Additionally, the seaside site showed higher signal

https://doi.org/10.5194/egusphere-2025-2042
Preprint. Discussion started: 11 August 2025

intensities of Reduced-sulfur compounds, primarily owing to the identification of abundant $C_nH_{2n-4}O_xS$ and $C_nH_{2n+2}O_xS$ homologues.

3.3 Case study: Evolution of molecular compositions

To investigate the impact of atmospheric processes on organic molecular composition, we selected two distinct episodes with significant increases in $PM_{2.5}$ concentrations (Case 1: March 26–29; Case 2: April 10–13) for further analysis (Fig. S10). In Case 1, the daily average offline $PM_{2.5}$ concentration increased from 27.35 to 38.80 μg m^{-3} at the urban site and from 27.37 to 45.89 μg m^{-3} at the seaside site. While in Case 2, it increased from 17.13 to 59.78 μg m^{-3} at the urban site and from 17.11 to 40.63 μg m^{-3} at the seaside site. Backward trajectory analysis (Fig. S11) revealed that the air masses in Case 1 were transported from North China along the coastline to study area over a long distance and then shifted to local air masses. This transport pattern was accompanied by initially elevated nighttime O_3 concentrations under regional influence, followed by a significant rise in NO*x* levels due to local accumulation. RH in Case 1 remained relatively stable at both sites, averaging approximately 72% (urban) and 86% (seaside). In contrast, the air masses in Case 2 were primarily influenced by long-range marine transport. The O*x* levels displayed repetitive and stable diurnal variations. Notably, RH progressively increased from 66% to 91% at the urban site and from 76% to 99% at the seaside site, while UVB intensity declined gradually from 12.6 to 5.4 w m^{-2} at the urban site and from 12.4 to 8.7 w m^{-2} at the seaside site. We also observed that as Case 2 progressed, the NO_3^- and SO_4^{2-} concentrations increased markedly with rising RH. Overall, the two episodes exhibited distinct source origins and environmental conditions.

The evolution of daily CHOX signal intensity during pollution episodes is presented in Fig.5. Case 1 exhibited higher CHOX signal intensities than Case 2. Spatially, the urban site showed higher levels of CHO and CHON compounds, while the seaside site had relatively higher concentrations of S-containing compounds, consistent with the general characteristics of the two sites. During Case 1, all CHOX compounds showed increased signal intensities, particularly urban CHON and seaside

https://doi.org/10.5194/egusphere-2025-2042
Preprint. Discussion started: 11 August 2025

S-containing compounds (Fig. 5b–d). This feature aligns with the earlier hypothesis that local emissions dominantly contributed to CHOX in this episode. As expected, NO*x* concentrations were significantly higher at the urban site (38.21 μg m^{-3}) than at the seaside site (24.91 μg m^{-3}), while SO_2 levels exhibited an inverse trend (urban: 3.29 μg m^{-3}; seaside: 4.54 μg m^{-3}). In contrast, Case 2 (Fig. 5b–d) was characterized by a significant temporal increase in CHO compounds, while CHON levels remained stable. Additionally, S-containing compounds showed a slight but synchronized enhancement at both sites, likely due to the influence of a common marine air mass source. Given the more pronounced variations in CHOX composition at the urban site, we conducted further analysis on CHOX at this location.

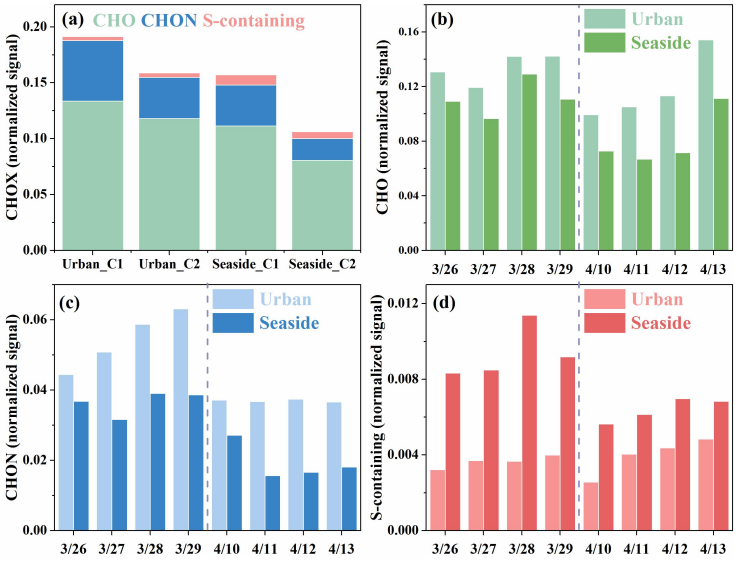

Fig. 5 Signal intensity of CHOX during the different periods at the two sites.

Figure 6 illustrates the compositional changes of CHOX compounds during the two pollution episodes. The OSc (0.37) of CHOX in Case 1 was significantly lower than the campaign average (0.49). Regarding CHOX composition, as the dominant influence shifted from long-distance transport to local accumulation, the proportion of Aliphatic-like O-rich components in CHOX decreased, while Aliphatic-like O-poor components contributed increasingly. These observations reflect the enhanced influence from local anthropogenic emissions. Our aforementioned results have

https://doi.org/10.5194/egusphere-2025-2042
Preprint. Discussion started: 11 August 2025

shown a significant enhancement of CHON signals in Case 1. Further compositional analysis revealed that as the episode progressed, the proportion of NACs (DBE<6) in CHON compounds decreased, accompanied by a modest increase in Aliphatic Nitrates. Figures 7a-d (marked by blue dashed boxes) specifically show that the urban CHON signal enhancement was primarily driven by low DBE/C compounds, including $C_{10}H_{19}NO_5$, $C_{10}H_{15}NO_6$, $C_4H_7NO_3$, $C_6H_{11}NO_6$, and $C_3H_7NO_3$. These organonitrates can be formed through daytime reactions between NO and organic peroxy radicals (generated from monoterpene oxidation by OH radicals or O_3), or via nighttime NO_3 radical-initiated reactions with monoterpenes (Atkinson and Arey, 2003; Kurten et al., 2017; Yan et al., 2016). During Case 1, elevated O_3 concentrations resulting from regional transport (Fig. S10a) likely facilitated nocturnal NO_3 radical formation via reactions with locally emitted NO_2. Online CIMS measurements also revealed that N_2O_5 signals in Case 1 were one order of magnitude higher than in Case 2 (data not shown). Together, these findings suggest that NO_3 radical-initiated nighttime reactions promoted the formation of Aliphatic Nitrates (e.g., $C_{10}H_{19}NO_5$ and $C_{10}H_{15}NO_6$) in CHON compounds during this stagnation events.

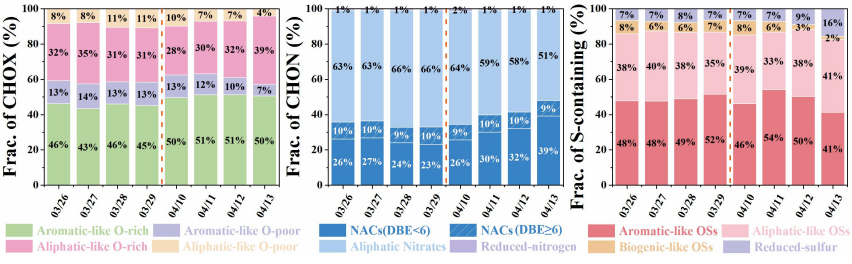

Fig. 6 Fraction distribution of urban CHOX signal intensity categorized by different parameter (AI_{mod}, DBE，H/C, and O/C) during Case 1 and Case 2.

Case 2 exhibited distinct characteristics compared to Case1 (Fig. 6). The OSc (0.51) of CHOX compounds in Case 2 was increased in contrast to the campaign average (0.49). The proportion of Aliphatic-like O-rich compounds demonstrated a continuous upward trend, rising from 28% to 39% at the urban site, while Aromatic-like O-rich compounds remained stable. Conversely, the proportion of both Aromatic-like O-poor and Aliphatic-like O-poor compounds decreased. Unlike CHO

https://doi.org/10.5194/egusphere-2025-2042
Preprint. Discussion started: 11 August 2025

compounds, the total signal intensities of CHON compounds in Case 2 remained relatively constant (Fig. 5c), but their molecular composition underwent significant changes. Specifically, the proportion of NACs (DBE<6) in CHON compounds increased from 26% to 39% at the urban site, whereas Aliphatic Nitrates decreased correspondingly from 64% to 51%. Additionally, variations in S-containing compounds were generally consistent across both sites (Fig. S12), with the most notable increases observed in Aliphatic-like OSs and Reduced sulfur compounds.

A distinct characteristic of Case 2 was the increased signal intensity of CHO compounds (Fig. 5b), particularly on April 13. The VK diagrams (Fig. 7i–l) showed that CHO compounds evolved into highly oxidized species (e.g., $C_2H_2O_4$, $C_4H_6O_4$, $C_5H_8O_4$) as aerosol concentrations increased. Previous studies have demonstrated that organic acids are continuously generated during aqueous photochemical aging processes (Ervens et al., 2011; Ye et al., 2025). The $C_nH_{2n-2}O_4$ homologues, such as $C_4H_6O_4$ (succinic acid) and $C_3H_4O_4$ (malonic acid), were predominantly formed via aqueous-phase reactions and/or photochemical oxidation of VOCs (Kawamura et al., 2016). The $C_5H_8O_4$ species likely represents glutaric acid, a known oxidation product of isoprene (Berndt et al., 2019). Research indicates that aqueous-phase reactions play a crucial role in generating highly oxidized OA (Xu et al., 2017b). We therefore infer that the increased RH under marine air mass influence during Case 2 promoted aqueous reaction-driven organic aerosol formation, thereby enhancing OA oxidation levels. This interpretation is supported by the observation that CHO compounds at the seaside site exhibited higher oxidation degrees than those at the urban site (Table S2). Regarding CHON compositional changes, the VK diagrams clearly showed a decline in signals from low DBE/C species (e.g., $C_{10}H_{19}NO_5$, $C_{10}H_{15}NO_6$, and $C_{10}H_{17}NO_6$, blue dashed box in Fig. 7e-h) alongside an increase in oxygen-rich and lower-carbon species (e.g., $C_6H_5NO_3$, $C_5H_3NO_3$, $C_3H_5NO_6$, $C_5H_5NO_6$, and $C_5H_9NO_6$, orange dashed box in Fig. 7e-h). These CHON compounds most likely originated from aromatic hydrocarbon oxidation followed by atmospheric aging processes, leading to concurrent increases in both weighted-AI_{mod} (0.16 vs. 0.14) and weighted-OSc (0.02

https://doi.org/10.5194/egusphere-2025-2042
Preprint. Discussion started: 11 August 2025

vs. -0.08). Overall, the compositional evolution in Case 2 demonstrates that marine-derived humid air masses enhanced aqueous-phase reactions, thereby promoting organic aerosol formation and intensifying oxidative states.

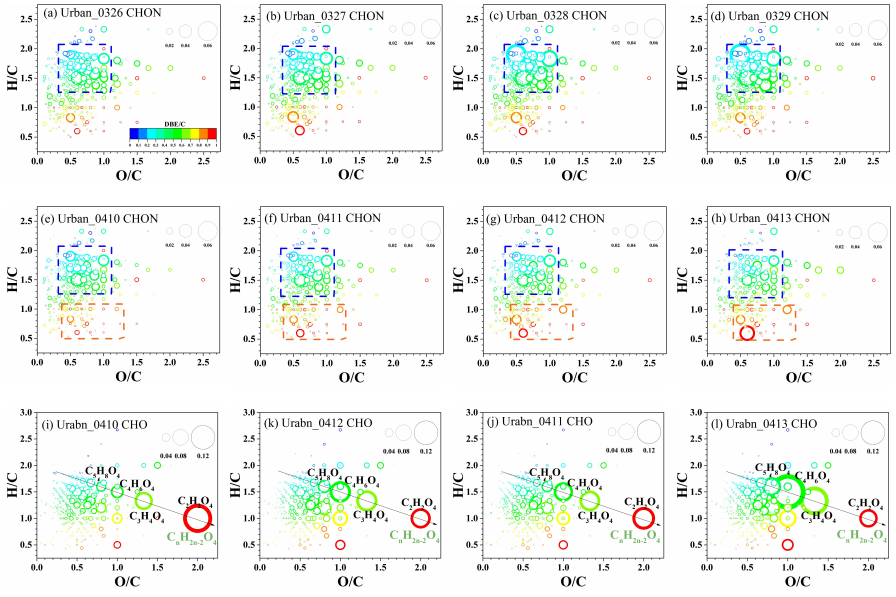

Fig. 7 The van Krevelen (VK) diagram of urban CHON (a–h) and CHO (i–l) day by day during different periods. The circle size corresponds to signal intensity and the color scale represents the DBE/C ratio. The low DBE/C ratio species are marked in the blue dashed box. The oxygen-rich and lower-carbon species are marked in the orange dashed box.

4 Conclusions

This study investigates the molecular characteristics and chemical evolution of OA in coastal environments (urban and seaside sites) through FIGAERO-I-CIMS analysis of $PM_{2.5}$ samples collected during spring 2024. CHO and CHON compounds dominated the OA composition at both sites, sharing over 50% of molecular formulas and accounting for 86%–94% of total signal intensities. The urban site exhibited higher signal intensities of CHON compounds, while the seaside site showed elevated S-containing compounds. These results clearly reflect distinct source-specific molecular fingerprints. The O_{eff}/C values (urban 0.82; seaside 0.85) indicated higher oxidation levels in coastal CHOX compounds. Compared to urban OA, Seaside OA

https://doi.org/10.5194/egusphere-2025-2042
Preprint. Discussion started: 11 August 2025

exhibited lower unsaturation, reduced aromaticity, and higher oxidation states. Categorization showed that Aromatic-like CHOX exhibited higher signals than Aliphatic-like compounds at both sites, while urban OA was enriched in aromatic species (e.g., NACs from vehicle- and combustion-related emissions) and seaside OA featured aliphatic and highly oxidized compounds. Two pollution episodes were selected to investigate CHOX evolution mechanisms. Case 1 (local accumulation) exhibited a significant increase in urban CHON compounds, likely resulting from NO_3·-initiated nighttime oxidation that promoted the formation of Aliphatic Nitrates under local NO*x* accumulation. Case 2 (marine air masses) showed increased proportions of Aliphatic-like O-rich CHOX compounds (28% to 39%) via aqueous-phase processing under high humidity. The offline FIGAERO-I-CIMS proved robust for molecular-level characterization of OA across diverse environments. These findings not only advance our understanding of OA molecular characteristics and chemical evolution processes, but also provide insights for region-specific control strategies.

CRediT authorship contribution statement

YC conducted the laboratory experiments. YC and LX analyzed the data and wrote the paper. ZL, CY, GC, RZ, and YZ coordinated the measurements and maintained data. LX, XF, and JC designed the project. JC, YH, and ML supervised the study. All the co-authors contributed to the discussion and commented on the manuscript.

Declaration of Competing Interest

The authors declare that they have no known competing financial interests or personal relationships that could have appeared to influence the work reported in this paper.

Data availability

The data related to this article are accessible at figshare (https://doi.org/10.6084/m9.figshare.28956629, Chen et al., 2025).

https://doi.org/10.5194/egusphere-2025-2042
Preprint. Discussion started: 11 August 2025

Acknowledgements

This study was funded by the National Natural Science Foundation of China (U22A20578 and 42277091), the National Key Research and Development Program (2022YFC3700304), the Science and Technology Department of Fujian Province (2022L3025), the guiding project of seizing the commanding heights of "self-purifying city" (no. IUE-CERAE-202402), STS Plan Supporting Project of the Chinese Academy of Sciences in Fujian Province (2023T3013), and Xiamen Atmospheric Environment Observation and Research Station of Fujian Province.

Reference

An, Y., Xu, J., Feng, L., Zhang, X., Liu, Y., Kang, S., Jiang, B., and Liao, Y.: Molecular characterization of organic aerosol in the Himalayas: insight from ultra-high-resolution mass spectrometry. Atmos. Chem. Phys., 19, 111-1128. doi:10.5194/acp-19-1115-2019, 2019.

Atkinson, R. and Arey, J.: Atmospheric degradation of volatile organic compounds. Chem. Rev., 103, 4605-4638. doi:10.1021/cr0206420, 2003.

Berndt, T., Hyttinen, N., Herrmann, H., and Hansel A.: First oxidation products from the reaction of hydroxyl radicals with isoprene for pristine environmental conditions. Commun. Chem., 2, 21. doi:10.1038/s42004-019-0120-9, 2019.

Bianchi, F., Kurten, T., Riva, M., Mohr, C., Rissanen, M., Roldin, P., Berndt, T., Crounse, J., Wennberg, P., Mentel, T., Wildt, J., Junninen, H., Jokinen, T., Kulmala, M., Worsnop, D., Thornton, J., Donahue, N., Kjaergaard, H., and Ehn, M. Highly oxygenated organic molecules (HOM) from gas-phase autoxidation involving peroxy radicals: A key contributor to atmospheric aerosol. Chem. Rev., 119 (6), 3472-509. doi:10.1021/acs.chemrev.8b00395, 2019.

Bianchi, F., Sinclair, V. A., Aliaga, D., Zha, Q., Scholz, W., Wu, C., Heikkinen, L., Modini, R., Partoll, E., Velarde, F., Moreno, I., Gramlich, Y., Huang, W., Leiminger, M., Enroth, J., Peräkylä, O., Marinoni, A., Xuemeng, C., Blacutt, L., Forno, R., Gutierrez, R., Ginot, P., Uzu, G., Facchini, M. C., Gilardoni, S., GyselBeer, M., Cai, R., Petäjä, T., Rinaldi, M., Saathoff, H., Sellegri, K., Worsnop, D., Artaxo, P., Hansel, A., Kulmala, M., Wiedensohler, A., Laj, P., Krejci, R., Carbone, S., Andrade, M., and Mohr, C.: The SALTENA Experiment: Comprehensive Observations of Aerosol Sources, Formation, and Processes in the South American Andes, B. Am. Meteorol. Soc., 103, E212-E229, doi:10.1175/BAMS-D-20-0187.1, 2022.

Brege, M., Paglione, M., Gilardoni, S., Decesari, S., Facchini, M. C., and Mazzoleni, L. R.: Molecular insights on aging and aqueous-phase processing from ambient biomass burning

https://doi.org/10.5194/egusphere-2025-2042
Preprint. Discussion started: 11 August 2025

emissions-influenced Po Valley fog and aerosol. Atmos. Chem. Phys., 18, 13197-13214. doi:10.5194/acp-18-13197-2018, 2018.

Boyd, C., Sanchez, J., Xu, L., Eugene, A., Nah, T., Tuet, W., Guzman, M., and Ng, N.: Secondary organic aerosol formation from the β-pinene+NO_3 system: effect of humidity and peroxy radical fate. Atmos. Chem. Phys., 15, 7497–7522. doi:10.5194/acp-15-7497-2015, 2015.

Cai, J., Wu, C., Wang, J., Du, W., Zheng, F., Hakala, S., Fan, X., Chu, B., Yao, L., Feng, Z., Liu, Y., Sun, Y., Zheng, J., Yan, C., Bianchi, F., Kulmala, M., Mohr, C., and Daellenbach, K. R.: Influence of organic aerosol molecular composition on particle absorptive properties in autumn Beijing. Atmos. Chem. Phys., 22, 1251–1269. doi:10.5194/acp-22-1251-2022, 2022.

Cai, J., Daellenbach, K. R., Wu, C., Zheng, Y., Zheng, F., Du, W., Haslett, S. L., Chen, Q., Kulmala, M., and Mohr, C.: Characterization of offline analysis of particulate matter with FIGAERO-CIMS. Atmos. Meas. Tech., 16, 1147–1165. doi:10.5194/amt-16-1147-2023, 2023.

Chan, M., Surratt, J., Chan, A., Schilling, K., Offenberg, J., Lewandowski, M., Edney, E., Kleindienst, T., Jaoui, M., Edgerton, E., Tanner, R., Shaw, S., Zheng, M., Knipping, E., and Seinfeld, J.: Influence of aerosol acidity on the chemical composition of secondary organic aerosol from β-caryophyllene. Atmos. Chem. Phys., 11, 1735-1751. doi:10.5194/acp-11-1735-2011, 2011.

Chazeau, B., Temime-Roussel, B., Gille, G., Mesbah, B., D'Anna, B., Wortham, H., and Marchand, N.: Measurement report: Fourteen months of real-time characterisation of the submicronic aerosol and its atmospheric dynamics at the Marseille–Longchamp supersite. Atmos. Chem. Phys. 21 (9), 7293-7319. doi:10.5194/acp-21-7293-2021, 2021.

Chen, G., Xu, L., Yu, S., Xue, L., Lin, Z., Yang, C., Ji, X., Fan, X., Tham, Y., Wang, H., Hong, Y., Li, M., Seinfeld, J., and Chen, J.: Increasing Contribution of Chlorine Chemistry to Wintertime Ozone Formation Promoted by Enhanced Nitrogen Chemistry. Environ. Sci. Technol., 58, 51, 22714-22721. doi:10.1021/acs.est.4c09523, 2024.

Chen, Y., Cao, J., Zhao, J., Xu, H., Arimoto, R., Wang, G., Han, Y., Shen, Z., Li, G.: N-alkanes and polycyclic aromatic hydrocarbons in total suspended particulates from the southeastern Tibetan Plateau: concentrations, seasonal variations, and sources. Sci. Total Environ., 470-471, 9-18. doi:10.1016/j. scitotenv.2013.09.033, 2014.

Chen, Y., Takeuchi, M., Nah, T., Xu, L., Canagaratna, M. R., Stark, H., Baumann, K., Canonaco, F., Prévôt, A. S. H., Huey, L. G., Weber, R. J., and Ng, N. L.: Chemical characterization of secondary organic aerosol at a rural site in the southeastern US: insights from simultaneous high-resolution time-of-flight aerosol mass spectrometer (HR-ToF-AMS) and FIGAERO chemical ionization mass spectrometer (CIMS) measurements. Atmos. Chem. Phys., 20, 8421-8440. doi:10.5194/acp-20-8421-2020, 2020.

Chen, Y., Yang, C., Xu, L., Chen, J., Zhang, Y., Shi, J., Fan, X., Zheng, R., Hong, Y., and Li, M.: Chemical composition of NR-PM_1 in a coastal city of Southeast China: Temporal variations and formation pathways. Atmos. Environ., 285. doi:10.1016/j.atmosenv.2022.119243, 2022.

https://doi.org/10.5194/egusphere-2025-2042
Preprint. Discussion started: 11 August 2025

659 Chen, Y., Xu, L., Fan, X., Lin, Z., Yang, C., Chen, G., Zheng, R., Hong, Y., Li, M., Zhang, Y., and
660 Chen, J.: Molecular characterization of organic aerosol between urban and seaside
661 environments using offline FIGAERO-I-CIMS, figshare [dataset],
662 https://doi.org/10.6084/m9.figshare.28956629.v1, 2025.

663 Chow, C., Watson, J., Lu, Z., Lowenthal, D., Frazier, C., Solomon, P., Thuillier, R., and Magliano,
664 K.: Descriptive analysis of $PM_{2.5}$ and PM_{10} at regionally representative locations during
665 SJVAQS/AUSPEX. Atmos. Environ., 30, 12, 2079-2112. doi:10.1016/1352-2310(95)00402-5,
666 1996.

667 Coward, E., Ohno, T., and Sparks, D.: Direct evidence for temporal molecular fractionation of
668 dissolved organic matter at the iron oxyhydroxide interface. Environ. Sci. Technol., 53 (2):
669 642-650. doi: 10.1021/acs.est. 8b04687, 2019.

670 Cui, M., Li, C., Chen, Y., Zhang, F., Li, J., Jiang, B., Mo, Y., Li, J., Yan, C., Zheng, M., Xie, Z.,
671 Zhang, G., and Zheng, J.: Molecular characterization of polar organic aerosol constituents in
672 offroad engine emissions using Fourier transform ion cyclotron resonance mass spectrometry
673 (FT-ICR MS): implications for source apportionment. Atmos. Chem. Phys., 19, 13945-13956.
674 doi:10.5194/acp-19-13945-2019, 2019.

675 Cui, M., Han, Y., Yan, C., Zhang, F., Li, J., and Chen, Y.: Characteristics of polar organic
676 compounds from diesel truck emissions measured by FT-ICR MS. Atmos. Environ., 319,
677 120319. doi:10.1016/j.atmosenv.2023.120319, 2024.

678 Daellenbach, K., Cai, j., Hakala, S., Dada, L., Yan, C., Du, W., Yao, L., Zheng, F., Ma, J.,
679 Ungeheuer, F., Vogel, A., Stolzenburg, D., Hao, Y., Liu, Y., Bianchi, F., Uzu, G., Jaffrezo, J.,
680 Worsnop, D., Donahue N., and Kulmala, M.: Substantial contribution of transported
681 emissions to organic aerosol in Beijing. Nat. Geosci., 17, 747-754.
682 doi:10.1038/s41561-024-01493-3, 2024.

683 Du, M., Voliotis, A., Shao, Y., Wang, Y., Bannan, T. J., Pereira, K. L., Hamilton, J. F., Percival, C.
684 J., Alfarra, M. R., and McFiggans, G.: Combined application of online FIGAERO-CIMS and
685 offline LC-Orbitrap mass spectrometry (MS) to characterize the chemical composition of
686 secondary organic aerosol (SOA) in smog chamber studies. Atmos. Meas. Tech., 15,
687 4385-4406. doi:10.5194/amt-15-4385-2022, 2022.

688 Du, Y., Che, H., Bao, Z., Liu, Y., Li, Q., Hu, M., Zhou, J., Zhang, S., Yao, X., Shi, Q., Chen, C.,
689 Han, Y., Meng, L., Long, X., Qi, X., He, C., and Chen, Y.: Characterization of Organosulfates
690 (OSs) in typical urban areas in Eastern China: Source, Process, and Volatility. Atmos. Res.,
691 301, 107258. doi:10.1016/j.atmosres.2024.107258, 2024.

692 Ervens, B., Turpin, B. J., and Weber, R. J.: Secondary organic aerosol formation in cloud droplets
693 and aqueous particles (aqSOA): a review of laboratory, field and model studies. Atmos.
694 Chem. Phys., 11, 11069–11102. doi:10.5194/acp-11-11069-2011, 2011.

695 Faxon, C., Hammes, J., Breton, M., Pathak, R., and Hallquist, M.: Characterization of organic
696 nitrate constituents of secondary organic aerosol (SOA) from nitrate-radical-initiated
697 oxidation of limonene using high-resolution chemical ionization mass spectrometry. Atmos.

https://doi.org/10.5194/egusphere-2025-2042
Preprint. Discussion started: 11 August 2025

Chem. Phys., 18, 5467–5481. doi:10.5194/acp-18-5467-2018, 2018.

Gallimore, P., Giorio, C., Mahon, B., and Kalberer, M.: Online molecular characterisation of organic aerosols in an atmospheric chamber using extractive electrospray ionisation mass spectrometry. Atmos. Chem. Phys., 17, 14485-14500, do:10.5194/acp-17-14485-2017, 2017.

Haslett, S. L., Bell, D. M., Kumar, V., Slowik, J. G., Wang, D. S., Mishra, S., Rastogi, N., Singh, A., Ganguly, D., Thornton, J., Zheng, F., Li, Y., Nie, W., Liu, Y., Ma, W., Yan, C., Kulmala, M., Daellenbach, K. R., Hadden, D., Baltensperger, U., Prevot, A. S. H., Tripathi, S. N., and Mohr, C.: Nighttime NO emissions strongly suppress chlorine and nitrate radical formation during the winter in Delhi. Atmos. Chem. Phys., 23, 9023-9036. doi:10.5194/acp-23-9023-2023, 2023.

Hong, Y., Xu, X., Liao, D., Liu, T., Ji, X., Xu, K., Liao, C., Wang, T., Lin, C., and Chen, J.: Measurement report: Effects of anthropogenic emissions and environmental factors on the formation of biogenic secondary organic aerosol (BSOA) in a coastal city of southeastern China. Atmos. Chem. Phys., 22, 7827-7841. doi:10.5194/acp-22-7827-2022, 2022.

Hong, Z., Zhang, H., Zhang, Y., Xu, L., Liu, T., Xiao, H., Hong, Y., Chen, J., Li, M., Deng, J., Wu, X., Hu, B., and Chen, X.: Secondary organic aerosol of $PM_{2.5}$ in a mountainous forest area in southeastern China: Molecular compositions and tracers implication. Sci. Total Environ., 653, 496-503. doi:10.1016/j.scitotenv.2018.10.370, 2019.

Huang, R. J., Zhang, Y., Bozzetti, C., Ho, K. F., Cao, J. J., Han, Y., Daellenbach, K. R., Slowik, J. G., Platt, S. M., Canonaco, F., Zotter, P., Wolf, R., Pieber, S. M., Bruns, E. A., Crippa, M., Ciarelli, G., Piazzalunga, A., Schwikowski, M., Abbaszade, G., Schnelle-Kreis, J., Zimmermann, R., An, Z., Szidat, S., Baltensperger, U., El Haddad, I., and Prevot, A. S.: High secondary aerosol contribution to particulate pollution during haze events in China. Nature, 514 (7521), 218-22. doi:10.1038/nature13774, 2014.

Huang, W., Saathoff, H., Shen, X., Ramisetty, R., Leisner, T., and Mohr. C.: Seasonal characteristics of organic aerosol chemical composition and volatility in Stuttgart, Germany. Atmos. Chem. Phys., 19 (18), 11687-11700. doi: 10.5194/acp-19-11687-2019, 2019.

Huang, W., Wu, C., Gao, L., Gramlich, Y., Haslett, S. L., Thornton, J., Lopez-Hilfiker, F. D., Lee, B. H., Song, J., Saathoff, H., Shen, X., Ramisetty, R., Tripathi, S. N., Ganguly, D., Jiang, F., Vallon, M., Schobesberger, S., Yli-Juuti, T., and Mohr, C.: Variation in chemical composition and volatility of oxygenated organic aerosol in different rural, urban, and mountain environments. Atmos. Chem. Phys., 24, 2607-2624. doi:10.5194/acp-24-2607-2024, 2024.

Jiang, B., Kuang, B., Liang, Y., Zhang, J., Huang, X., Xu, C., Yu, J., and Shi, Q.: Molecular composition of urban organic aerosols onclear and hazy days in Beijing: a comparative study using FT-ICR MS. Environ. Chem., 13, 888-901. doi:10.1071/EN15230, 2016.

Junninen, H., Ehn, M., Petäjä, T., Luosujärvi, L., Kotiaho, T., Kostiainen, R., Rohner, U., Gonin, M., Fuhrer, K., Kulmala, M., and Worsnop, D. R.: A high-resolution mass spectrometer to measure atmospheric ion composition. Atmos. Meas. Tech., 3, 1039-1053. doi:10.5194/amt-3-1039-2010, 2010.

https://doi.org/10.5194/egusphere-2025-2042
Preprint. Discussion started: 11 August 2025

737 Kawamura, K. and Bikkina, S.: A review of dicarboxylic acids and related compounds in
738 atmospheric aerosols: Molecular distributions, sources and transformation. Atmos. Res., 170,
739 140-160. doi:10.1016/j.atmosres.2015.11.018, 2016.

740 Koch, B. and Dittmar, T.: From Mass to Structure: An Aromaticity Index for High-Resolution
741 Mass Data of Natural Organic Matter. Rapid Commun. Mass Spectrom., 20 (5), 926-932.
742 doi:10.1002/rcm.2386, 2006.

743 Koch, B. and Dittmar, T.: From Mass to Structure: An Aromaticity Index for High-Resolution
744 Mass Data of Natural Organic Matter. Rapid Commun. Mass Spectrom., 30 (1), 250.
745 doi:10.1002/rcm.7433, 2016.

746 Kroll, J., Donahue, N., Jimenez, J., Kessler, S., Canagaratna, M., Wilson, K., Altieri, K.,
747 Mazzoleni, L., Wozniak, A., Bluhm, H., Mysak, E., Smith, J., Kolb C., and Worsnop, D.:
748 Carbon Oxidation State as a Metric for Describing the Chemistry of Atmospheric Organic
749 Aerosol. Nat. Chem., 3, 133−139. doi:10.1038/nchem.948, 2011.

750 Kurten, T., Møller, K., Nguyen, T., Schwantes, R., Misztal, P., Su, L., Wennberg, P., Fry, J.,
751 Kjaergaard, H.: Alkoxy radical bond scissions explain the anomalously low secondary
752 organic aerosol and organonitrate yields from α-Pinene + NO_3. J. Phys. Chem. Lett., 8, 13,
753 2826-2834. doi:10.1021/acs.jpclett.7b01038, 2017.

754 Lee, B. H., Lopez-Hilfiker, F., Mohr, C., Kurten, T., Worsnop, D., and Thornton. J.: An
755 iodide-adduct high-resolution time-of-flight chemical-ionization mass spectrometer:
756 Application to atmospheric inorganic and organic compounds. Environ. Sci. Technol., 48 (11),
757 6309-6317. doi: 10.1021/es500362a, 2014.

758 Lim, Y. B., Tan, Y., Perri, M. J., Seitzinger, S. P., and TurpinB. J.: Aqueous chemistry and its role
759 in secondary organic aerosol (SOA) formation. Atmos. Chem. Phys., 10, 10521-10539.
760 doi:10.5194/acp-10-10521-2010, 2010.

761 Lin, P., Rincon, A., Kalberer, M., and Yu, J.: Elemental composition of HULIS in the Pearl River
762 Delta Region, China: Results inferred from positive and negative electrospray high resolution
763 mass spectrometric data. Environ. Sci. Technol., 46 (14):7454-7462. doi: 10.1021/ es300285d,
764 2012.

765 Lopez-Hilfiker, F. D., Mohr, C., Ehn, M., Rubach, F., Kleist, E., Wildt, J., Mentel, Th. F., Lutz, A.,
766 Hallquist, M., Worsnop, D., and Thornton, J. A.: A novel method for online analysis of gas
767 and particle composition: description and evaluation of a Filter Inlet for Gases and AEROsols
768 (FIGAERO). Atmos. Meas. Tech., 7, 983-1001. doi:10.5194/amt-7-983-2014, 2014.

769 Lopez-Hilfiker, F. D., Mohr, C., D'Ambro, E. L., Lutz, A., Riedel, T. P., Gaston, C. J., Iyer, S.,
770 Zhang, Z., Gold, A., Surratt, J. D., Lee, B. H., Kurten, T., Hu, W. W., Jimenez, J., Hallquist,
771 M., and Thornton, J. A.: Molecular composition and volatility of organic aerosol in the
772 Southeastern U.S.: Implications for IEPOX derived SOA. Environ. Sci. Technol., 50,
773 2200-2209. doi:10.1021/acs.est.5b04769, 2016.

774 Nguyen, T., Lee, P., Updyke, K., Bones, D., Laskin, J., Laskin, A., and Nizkorodov, S.: Formation

https://doi.org/10.5194/egusphere-2025-2042
Preprint. Discussion started: 11 August 2025

of nitrogen- and sulfur-containing light-absorbing compounds accelerated by evaporation of water from secondary organic aerosols. J. Geophys. Res. Atmos., 117. doi:10.1029/2011JD016944, 2012.

Ning, C., Gao, Y., Yang, H., and Hao, X.: Molecular characteristics and potential source of urban $PM_{2.5}$-bound water-soluble organic matter in Shanghai during springtime. Atmos. Environ., 311, 120025. doi:10.1016/j.atmosenv.2023.120025, 2023.

Noziere, B., Ekstrom, S., Alsberg, T., and Holmstrom, S.: Radical-initiated formation of organosulfates and surfactants in atmospheric aerosols. Geophys. Res. Lett., 37. doi:10.1029/2009GL041683, 2010.

Putman, A., Offenberg, J., Fisseha, R., Kundu, S., Rahn, T., and Mazzoleni, L.: Ultrahigh-resolution FT-ICR mass spectrometry characterization of α-pinene ozonolysis SOA. Atmos. Environ., 46, 164-172. doi.:10.1016/j.atmosenv.2011.10.003, 2012.

Qi, J., Zheng, B., Li, M., Yu, F., Chen, C., Liu, F., Zhou, X., Yuan, J., Zhang, Q., He, K.: A high-resolution air pollutants emission inventory in 2013 for the Beijing-Tianjin-Hebei region, China. Atmos. Environ., 170, 156-168. doi.:10.1016/j.atmosenv.2017.09.039, 2017.

Redman, A., Macalady, D., and Ahmann, D.: Natural organic matter affects arsenic speciation and sorption onto hematite. Environ. Sci. Technol., 36, 2889-2896. doi:10.1021/es0112801, 2002.

Shang, Y., Li,L., Sun, T., Kong, X., Wang, S., and Hallquist M.: Characterization and Seasonal Variation of $PM_{2.5}$ Composition in Xi'an, Northwest China: Oxygenated and Nitrogenous Organic Aerosol. ACS Earth Space Chem., 8, 1370-1384. doi:10.1021/acsearthspacechem.4c00042, 2024.

Siegel, K., Karlsson, L., Zieger, P., Baccarini, A., Schmale, J., Lawler, M., Salter, M., Leck, C., Ekman, A., Riipinen I., and Mohr, C.: Insights into the molecular composition of semivolatile aerosols in the summertime central Arctic Ocean using FIGAERO-CIMS. Environ. Sci.: Atmos., 1, 161. doi:10.1039/d0ea00023j, 2021.

Stark, H., Yatavelli, R. L. N., Thompson, S. L., Kang, H., Krechmer, J. E., Kimmel, J. R., Palm, B. B., Hu, W., Hayes, P. L., Day, D. A., Campuzano-Jost, P., Canagaratna, M. R., Jayne, J. T., Worsnop D. R., and Jimenez, J. L.: Impact of Thermal Decomposition on Thermal Desorption Instruments: Advantage of Thermogram Analysis for Quantifying Volatility Distributions of Organic Species. Environ. Sci. Technol., 51, 8491-8500. doi:10.1021/acs.est.7b00160, 2017.

Sun, Y., Xu, W., Zhang, Q., Jiang, Q., Canonaco, F., Prévôt, A. S. H., Fu, P., Li, J., Jayne, J., Worsnop, D. R., and Wang, Z.: Source apportionment of organic aerosol from 2-year highly time-resolved measurements by an aerosol chemical speciation monitor in Beijing, China. Atmos. Chem. Phys., 18 (12), 8469-8489. doi:10.5194/acp-18-8469-2018, 2018.

Wan, Y., Huang, X., Jiang, B., Kuang, B., Lin, M., Xia, D., Liao, Y., Chen, J., Yu, J. Z., and Yu, H.: Probing key organic substances driving new particle growth initiated by iodine nucleation in coastal atmosphere. Atmos. Chem. Phys., 20, 9821-9835. doi:10.5194/acp-20-9821-2020,

https://doi.org/10.5194/egusphere-2025-2042
Preprint. Discussion started: 11 August 2025

2020.

Xu, L., Guo, H., Weber R. J., and Ng, N. L.: Chemical Characterization of Water-Soluble Organic Aerosol in Contrasting Rural and Urban Environments in the Southeastern United States. Environ. Sci. Technol., 51, 78-88. doi:10.1021/acs.est.6b05002, 2017a.

Xu, W., Han, T., Du, W., Wang, Q., Chen, C., Zhao, J., Zhang, Y., Li, J., Fu, P., Wang, Z., Worsnop, D., and Sun, Y.: Effects of Aqueous-Phase and Photochemical Processing on Secondary Organic Aerosol Formation and Evolution in Beijing, China. Environ. Sci. Technol., 51, 762-770. doi:10.1021/acs.est.6b04498, 2017b.

Xu, W., Kuang, Y., Liang, L.., He, Y., Cheng, H., Bian, Y., Tao, J., Zhang, G., Zhao, P., Ma, N., Zhao, H., Zhou, G., Su, H., Cheng, Y., Xu, X., Shao, M., Sun, Y.: Dust-dominated coarse particles as a medium for rapid secondary organic and inorganic aerosol formation in highly polluted air. Environ. Sci. Technol., 54, 15710-15721. doi:0.1021/acs.est.0c07243, 2020.

Xie, Q., Li, Y., Yue, S., Su, S., Cao, D., Xu, Y., Chen, J., Tong, H., Su, H., Cheng, Y., Zhao, W., Hu, W., Wang, Z., Yang, T., Pan, X., Sun, Y., Wang, Z., Liu, C., Kawamura, K., Jiang, G., Shiraiwa, M., Fu P.: Increase of high molecular weight organosulfate with intensifying urban air pollution in the Megacity Beijing. J. Geophys. Res. Atmos., 125(10):e2019JD032200. doi:10.1029/2019JD032200, 2020.

Xin, X., Zhao, Y., Wan, Y., Zhang H., and Yu, H.: Molecular composition of organic aerosols in urban and marine atmosphere: A comparison study using FIGAERO-I-CIMS, ESI-FT-ICR MS, and GC × GC-EI-ToF-MS. Aerosol Sci. and Tech., 58(10), 1142-1156. doi:10.1080/02786826.2024.2377394, 2024.

Yan, C., Nie, W., Äijälä, M., Rissanen, M. P., Canagaratna, M. R., Massoli, P., Junninen, H., Jokinen, T., Sarnela, N., Häme, S. A. K., Schobesberger, S., Canonaco, F., Yao, L., Prévôt, A. S. H., Petäjä, T., Kulmala, M., Sipilä, M., Worsnop, D. R., and Ehn, M.: Source characterization of highly oxidized multifunctional compounds in a boreal forest environment using positive matrix factorization. Atmos. Chem. Phys., 16, 12715-12731. doi:10.5194/acp-16-12715-2016, 2016.

Ye, C., Yuan, B., Lin, Y., Wang, Z., Hu, W., Li, T., Chen, W., Wu, C., Wang, C., Huang, S., Qi, J., Wang, B., Wang, C., Song, W., Wang, X., Zheng, E., Krechmer, J. E., Ye, P., Zhang, Z., Wang, X., Worsnop, D. R., and Shao, M.: Chemical characterization of oxygenated organic compounds in the gas phase and particle phase using iodide CIMS with FIGAERO in urban air. Atmos. Chem. Phys., 21, 8455-8478. doi:10.5194/acp-21-8455-2021, 2021.

Ye, Z., Hu, D., Wang, Z., Wang, H., and Ge, X.: Aqueous photochemical aging of water-soluble smoke particles from crop straws burning. Atmos. Environ., 40, 120897. doi:10.1016/j.atmosenv.2024.120897, 2025.

Yu, L., Smith, J., Laskin, A., George, K. M., Anastasio, C., Laskin, J., Dillner A. M., and Zhang, Q.: Molecular transformations of phenolic SOA during photochemical aging in the aqueous phase: competition among oligomerization, functionalization, and fragmentation, Atmos. Chem. Phys., 16, 4511-4527. doi:10.5194/acp-16-4511-2016, 2016.

https://doi.org/10.5194/egusphere-2025-2042
Preprint. Discussion started: 11 August 2025

852 Zhang, M., Cai, D., Lin, Z., Liu, Z., Li, M., Wang, Y., and Chen, J.: Molecular characterization of
853 atmospheric organic aerosols in typical megacities in China. npj Clim. Atmos. Sci., 7, 230.
854 doi:10.1038/s41612-024-00784-1, 2024.

855 Zhang, Y., Xu, L., Zhuang, M., Zhao, G., Chen, Y., Tong, L., Yang, C., Xiao, H., Chen, J., Wu, X.,
856 Hong, Y., Li, M., Bian, Y., and Chen, Y.: Chemical composition and sources of submicron
857 aerosol in a coastal city of China: Results from the 2017 BRICS summit study. Sci. Total
858 Environ., 741, 140470. doi:10.1016/j.scitotenv.2020.140470, 2020.

859 Zhao, R., Mungall, E. L., Lee, A. K. Y., Aljawhary, D., and Abbatt, J. P. D.: Aqueous-phase
860 photooxidation of levoglucosan-a mechanistic study using aerosol time-of-flight chemical
861 ionization mass spectrometry (Aerosol ToF-CIMS). Atmos. Chem. Phys., 14, 9695-9706.
862 doi:10.5194/acp-14-9695-2014, 2014.

863 Zheng, Y., Chen, Q., Cheng, X., Mohr, C., Cai, J., Huang, W., Shrivastava, M., Ye, P., Fu, P., Shi,
864 X., Ge, Y., Liao, K., Miao, R., Qiu, X., Koenig, T., and Chen S.: Precursors and Pathways
865 Leading to Enhanced Secondary Organic Aerosol Formation during Severe Haze Episodes.
866 Environ. Sci. Technol., 55, 15680-15693. doi:10.1021/acs.est.1c04255, 2021.

867 Zhou, W., Xu, W., Kim, H., Zhang, Q., Fu, P., Worsnop, D. R., and Sun, Y.: A review of aerosol
868 chemistry in Asia: insights from aerosol mass spectrometer measurements. Environ. Sci.
869 Process Impacts, 22 (8), 1616-1653. doi:10.1039/d0em00212g, 2020.